PHYSICAL REVIEW D **86,** 104001 (2012)

New code for equilibriums and quasiequilibrium initial data of compact objects. II. Convergence tests and comparisons of binary black hole initial data

Kōji Uryū,[1,*] Antonios Tsokaros,[2,†] and Philippe Grandclément[3,‡]

[1]*Department of Physics, University of the Ryukyus, Senbaru, Nishihara, Okinawa 903-0213, Japan*
[2]*Department of I.C.S.E., University of Aegean, Karlovassi 83200, Samos, Greece*
[3]*Laboratoire Univers et Théories, UMR 8102 du CNRS, Observatoire de Paris, Université Paris Diderot, F-92190 Meudon, France*

(Received 27 July 2012; published 1 November 2012)

COCAL is a code for computing equilibriums or quasiequilibrium initial data of single or binary compact objects based on finite difference methods. We present the results of supplementary convergence tests of COCAL code using time symmetric binary black hole data (Brill-Lindquist solution). Then, we compare the initial data of binary black holes on the conformally flat spatial slice obtained from COCAL and KADATH, where KADATH is a library for solving a wide class of problems in theoretical physics including relativistic compact objects with spectral methods. Data calculated from the two codes converge nicely towards each other, for close as well as largely separated circular orbits of binary black holes. Finally, as an example, a sequence of equal mass binary black hole initial data with corotating spins is calculated and compared with data in the literature.

DOI: 10.1103/PhysRevD.86.104001 PACS numbers: 04.25.D−, 04.25.dg, 04.30.Db, 04.40.Dg

I. INTRODUCTION

Various methods have been developed in the past couple of decades for computing numerical solutions of compact objects in equilibrium or quasiequilibrium. Those include methods for computing relativistic rotating stars in equilibrium or binary black hole initial data (see e.g. [1,2]). For example, numerical solutions of binary black holes (BBH) in quasicircular orbits have been widely used for initial data of merger simulations [3,4], and sequences of such data with fixed irreducible mass of each black hole (BH) have been also applied to approximate the inspiral evolution of BBH [5].

The authors have been developing, independently, numerical codes for computing such compact objects, COCAL [6] (Paper I hereafter) and KADATH [7] (Paper II). COCAL is a code for computing various kinds of astrophysical compact objects—isolated or binary systems of neutron stars and black holes which may be associated with strong magnetic fields. KADATH is a library for solving a wide class of problems in theoretical physics including those of general relativity, and is capable of computing such compact objects.

In the first part of this paper, we present the results of supplementary convergence tests of COCAL to those presented in Paper I. With straightforward changes in the radial coordinate grid spacings and in the finite difference formula for the integration over the zenith angle, errors in the gravitational fields especially near the compact objects decrease substantially, which is necessary to improve the accuracy of widely separated BBH solutions. In the second part of the paper, we carefully compare the spatially conformally flat BBH initial data in circular orbit calculated from COCAL and KADATH code. Comparison of the solutions is the most effective test to confirm the reliability of the codes in which a system of complicated equations is solved. Such comparison had been done for the codes for relativistic rotating stars in [8]. To our knowledge, this is the first attempt to compare the BBH data calculated from totally different methods as the spectral method and the finite difference method. Finally, we present a sequence of spatially conformally flat BBH initial data in circular orbits for the case with equal mass and corotating spin, and compare the result with those presented in [5]. Throughout the paper we use geometric units with $G = c = 1$.

II. CONVERGENCE TESTS FOR COCAL CODE

In this section, we present convergence tests of COCAL code supplementary to those presented in Paper I. The setup for the test problem is the same as in Paper I: the Brill-Lindquist solution for the time symmetric BBH data is generated numerically, and it is compared with the analytic value. We briefly review the setup of the problem and discuss the modification of the finite difference scheme from the previous paper.

A. A test problem for binary black holes

We assume the spacetime $\mathcal{M}$ is foliated by a family of spacelike hypersurfaces $(\Sigma_t)_{t\in\mathbb{R}}$, $\mathcal{M} = \mathbb{R}\times\Sigma$ parametrized by $t \in \mathbb{R}$. We assume the line element in the neighborhood of Σ_t to be

$$ds^2 = -\alpha^2 dt^2 + \psi^4 f_{ij} dx^i dx^j, \tag{1}$$

*uryu@sci.u-ryukyu.ac.jp
†atsok@aegean.gr
‡philippe.grandclement@obspm.fr

where f_{ij} is the flat spatial metric, so that the data on Σ_t becomes time symmetric—the extrinsic curvature K_{ab} on Σ_t vanishes.

Decomposing Einstein's equation $G_{\alpha\beta} = 0$ with respect to the foliation using hypersurface normal n^α to Σ_t, and the projection tensor $\gamma^{ab} = g^{\alpha\beta} + n^\alpha n^\beta$ to it, we write the Hamiltonian constraint $G_{\alpha\beta} n^\alpha n^\beta = 0$, and a combination of the spatial trace of Einstein's equation and the constraint $G_{\alpha\beta}(\gamma^{\alpha\beta} + \frac{1}{2} n^\alpha n^\beta) = 0$, as

$$\nabla^2 \psi = 0 \quad \text{and} \quad \nabla^2(\alpha\psi) = 0. \tag{2}$$

These equations have solutions, which correspond to the Schwarzschild metric in isotropic coordinates for a single BH. For a two BH case, a BBH solution is given by Brill and Lindquist [9]:

$$\psi = 1 + \frac{M_1}{2r_1} + \frac{M_2}{2r_2} \quad \text{and} \quad \alpha\psi = 1 - \frac{M_1}{2r_1} - \frac{M_2}{2r_2}, \tag{3}$$

where subscripts 1 and 2 correspond to those of the first and second BH; r_1 and r_2 are distances from the first and second BH, respectively, and M_1 and M_2 are mass parameters. Instead of solving two Laplace equations [Eq. (2)], we write an equation for α with a source on the whole domain of Σ_t:

$$\nabla^2 \psi = 0 \quad \text{and} \quad \nabla^2 \alpha = -\frac{2}{\psi} f^{ij} \partial_i \psi \, \partial_j \alpha. \tag{4}$$

In an actual computation, spherical regions near the center of BH are excised to avoid singularities. Therefore, boundary conditions for these elliptic equations are imposed at the radius $r = r_a$ of the excised sphere S_a, and at the radius $r = r_b$ of the boundary of computational domain S_b. We also set the mass parameters M_1 and M_2 as $0.8 \times r_a$ of each BH to avoid the lapse to be negative at S_a. In the following tests, we impose Dirichlet boundary conditions on S_a and S_b whose values are taken from the analytic solution (3).

B. Coordinates, grid setup, and finite difference scheme of COCAL code

As explained in Paper I, three spherical coordinate patches are introduced for solving binary compact objects with COCAL. Two of them are the compact objects coordinate patches (COCP-I and II) and one is the asymptotic region coordinate patch (ARCP). In each spherical patch, coordinates cover the region $(r, \theta, \phi) \in [r_a, r_b] \times [0, \pi] \times [0, 2\pi]$. The two COCPs are centered at the center of compact objects and extend up to about $r_b \sim O(10^2\ \mathrm{M})$, while ARCP is centered at the center of mass of the binary, and extends from $r_a \sim O(10\ \mathrm{M})$ to $r_b \sim O(10^6\ \mathrm{M})$, where M is the total mass of the system. Definitions of the parameters for the grid setups are listed in Table I.

In solving a system of elliptic equations such as Eq. (4), we rewrite them in integral form using Green's function that satisfies given boundary conditions, and apply a finite difference scheme to discretize those integral equations on the spherical coordinates of each domain. We use the midpoint rule for numerical quadrature formula, and hence compute the source terms at the midpoints of the grids. Coordinate grids (r_i, θ_j, ϕ_k) with $i = 0, \ldots, N_r$, $j = 0, \ldots, N_\theta$, and $k = 0, \ldots, N_\phi$, are freely specifiable except for the end point of each coordinate grid that corresponds to the boundary of the computational region, $(r_0, \theta_0, \phi_0) = (r_a, 0, 0)$ and $(r_{N_r}, \theta_{N_\theta}, \phi_{N_\phi}) = (r_b, \pi, 2\pi)$. The grid setup for COCP and ARCP is the same as Paper I except for the radial grid of COCP which will be explained later. For angular coordinate grids (θ_j, ϕ_k), we choose equally spaced grids.

In Paper I, we have used for the finite difference formulas, (1) 2nd order midpoint rule for the quadrature formula, (2) 2nd order finite difference formula for the θ and ϕ derivatives evaluated at the midpoints $(r_{i+\frac{1}{2}}, \theta_{j+\frac{1}{2}}, \phi_{k+\frac{1}{2}}) = ((r_i + r_{i+1})/2, (\theta_i + \theta_{i+1})/2, (\phi_i + \phi_{i+1})/2)$, (3) 3rd order finite difference formula for the r derivative evaluated at the midpoints, and (4) 4th order finite difference formula for the derivatives evaluated at the grid points, (r_i, θ_j, ϕ_k). In the present

TABLE I. Summary of grid parameters for COCP.

r_a: Radial coordinate where the radial grids start.
r_b: Radial coordinate where the radial grids end.
r_c: Radial coordinate between r_a and r_b where the radial grid spacing changes.
r_e: Radius of the excised sphere.
N_r: Number of intervals Δr_i in $r \in [r_a, r_b]$.
N_r^{f}: Number of intervals Δr_i in $r \in [r_a, 1]$.
N_r^{m}: Number of intervals Δr_i in $r \in [r_a, r_c]$.
N_θ: Number of intervals $\Delta\theta_j$ in $\theta \in [0, \pi]$.
N_ϕ: Number of intervals $\Delta\phi_k$ in $\phi \in [0, 2\pi]$.
d: Coordinate distance between the center of S_a ($r = 0$) and the center of mass.
d_s: Coordinate distance between the center of S_a ($r = 0$) and the center of S_e.
L: Order of included multipoles.

computations, we use the same finite difference formulas mentioned above except for the numerical quadrature formula in θ integrations.

Differences from the previous Paper I are the spacings of radial grids $\Delta r_i := r_i - r_{i-1}$ in COCP, and the quadrature formula used for the integration in zenith angle θ.

1. Radial grid spacings for COCP

When we compute a sequence of BBH data from larger to smaller separations in the COCAL code, we change the BH excision radius r_a from smaller to larger values and fix the separation d_s (instead of fixing r_a and varying d_s). In this way, the number of grid points are kept to be the same, and the structures of coordinate grids are almost the same for all solutions of the sequence. As a result the discretization error behaves systematically from one solution to the other, and hence the quantities such as mass or angular momentum vary smoothly along a sequence of solutions.

It is important to notice that, by changing the BH radius, we change the mass of the solution and hence change the length scale of the system. Therefore, to maintain the accuracy of the gravitational fields near the BH, the intervals near the hole should be proportional to the mass of the BH, or in our case, the BH excision radius r_a. Therefore, we modify the construction of the grid spacing in the radial direction r of COCP for computing a sequence from smaller to larger BH as follows. Without loss of generality, we set the radius of BH excision sphere S_a as $r_a < 1$. We divide the radial coordinate to four regions, I: $r \in [r_a, 1]$, II: $r \in [1, r_c]$, III: $r \in [r_c, 3r_c]$, and IV: $r \in [3r_c, r_b]$. We set the first interval by

$$\Delta r_1 = \frac{r_a}{\lambda N_r^{\rm f}}, \tag{5}$$

where $N_r^{\rm f}$ is the number of intervals in the region I: $[r_a, 1]$, and λ is a constant factor which is chosen to be $\lambda = 0.75$. For each region, $\Delta r_i := r_i - r_{i-1}$, are defined by

$$\Delta r_{i+1} = h_1 \Delta r_i, \qquad \text{for } i = 1, \ldots, N_r^{\rm f} - 1, \tag{6}$$

$$\Delta r_i = \Delta r, \qquad \text{for } i = N_r^{\rm f}, \ldots, N_r^{\rm m}, \tag{7}$$

$$\Delta r_{i+1} = h_3 \Delta r_i, \qquad \text{for } i = N_r^{\rm m}, \ldots, N_r^{\rm m} + N_r^{\rm f} - 1, \tag{8}$$

$$\Delta r_{i+1} = h_4 \Delta r_i, \qquad \text{for } i = N_r^{\rm m} + N_r^{\rm f}, \ldots, N_r - 1, \tag{9}$$

which correspond to regions I, II, III, and IV, respectively, The ratios $h_i (>1)$ $(i = 1, 3, 4)$ are respectively determined from relations

$$1 - r_a = \Delta r_1 \frac{h_1^{N_r^{\rm f}} - 1}{h_1 - 1}, \tag{10}$$

$$2r_c = \Delta r \frac{h_3 (h_3^{N_r^{\rm f}} - 1)}{h_3 - 1}, \tag{11}$$

$$r_b - 3r_c = \Delta r \frac{h_4 (h_4^{N_r - N_r^{\rm m} - N_r^{\rm f}} - 1)}{h_4 - 1}. \tag{12}$$

Values of the parameters for the coordinate grids of COCAL used in computing the results presented in this paper are listed in Table II. In Fig. 1, an example of the radial grid points is plotted for the case with H3 grid setup in Table II. Because of the construction, the grid structure in the region larger than $r \geq 1$ is the same for all solutions with different BH radius r_a once a grid setup (resolution) as in Table II is selected.

2. 4th order midpoint rule for the quadrature formula of θ integration

As discussed in Paper I, our Poisson solver is a system of integral equations, and it is numerically integrated with a quadrature formula of midpoint rule. Therefore, the sources of the integrals are always evaluated at the midpoints of (r_i, θ_j, ϕ_k) grids. As summarized above, the 2nd order midpoint rule was used for a quadrature formula in

TABLE II. Grid parameters of COCAL used for computation of BBH data. The separation of two BHs is fixed as $d_s = 2.5$. For the excision radius r_a for COCP-1 and 2, "var." stands for a variable parameter assigned to each solution. In the test problems in Sec. II C, they are chosen to be $r_a = 0.2$ and 0.4 for close BBH, and $r_a = 0.05$ and 0.1 for separated BBH for COCP-1 and 2, respectively.

Type	Patch	r_a	r_b	r_c	r_e	$N_r^{\rm f}$	$N_r^{\rm m}$	N_r	N_θ	N_ϕ	L
H1	COCP-1	var.	10^2	1.25	1.125	32	40	96	24	24	12
	COCP-2	var.	10^2	1.25	1.125	32	40	96	24	24	12
	ARCP	5.0	10^6	6.25	⋯	8	10	96	24	24	12
H2	COCP-1	var.	10^2	1.25	1.125	64	80	192	48	48	12
	COCP-2	var.	10^2	1.25	1.125	64	80	192	48	48	12
	ARCP	5.0	10^6	6.25	⋯	16	20	192	48	48	12
H3	COCP-1	var.	10^2	1.25	1.125	128	160	384	96	96	12
	COCP-2	var.	10^2	1.25	1.125	128	160	384	96	96	12
	ARCP	5.0	10^6	6.25	⋯	32	40	384	96	96	12
H4	COCP-1	var.	10^2	1.25	1.125	256	320	768	192	192	12
	COCP-2	var.	10^2	1.25	1.125	256	320	768	192	192	12
	ARCP	5.0	10^6	6.25	⋯	64	80	768	192	192	12

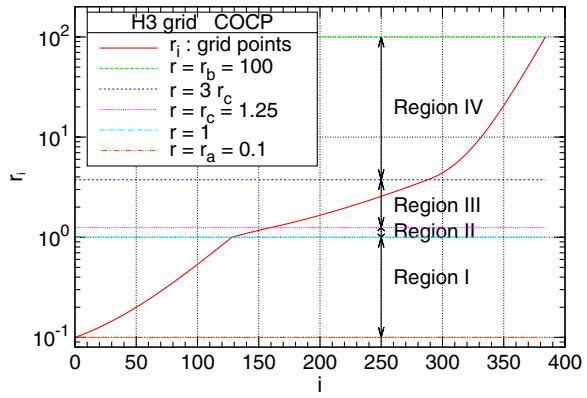

FIG. 1 (color online). The radial grid points r_i of COCP are plotted against the grid number $i = 0, \ldots, N_r$ for the case with H3 grid in Table II.

Paper I. With the above-mentioned choice for finite difference formulas, the 2nd order convergence of the error has been achieved. As shown in the top panel of Fig. 2 (as well as Figs. 3, 4, and 6 in Paper I), however, the fractional error of the potentials normally increases near the excision surfaces of the BH, S_a ($r = r_a$), although it converges in 2nd order.

One might expect that the increase of the error near S_a is due only to a lack of resolution in radial grid points. It turns out, however, that the finite difference errors in the potentials near the boundaries of computational domains are dominated by the discretization error in the θ coordinate. In particular, the θ integration of the source involving the Legendre function turns out to be the source of error. Therefore, we replace the quadrature formula of θ integration to 4th order accurate midpoint rule whose weights are

$$\int_{\theta_j}^{\theta_{j+4}} f(\theta) d\theta \simeq \Delta\theta \left(\frac{13}{12} f_{j+\frac{1}{2}} + \frac{11}{12} f_{j+\frac{3}{2}} + \frac{11}{12} f_{j+\frac{5}{2}} + \frac{13}{12} f_{j+\frac{7}{2}} \right), \tag{13}$$

where the grid number j is a multiple of 4, and $\Delta\theta = \pi/N_\theta$.

C. Convergence tests

We perform convergence tests to examine that the above two modifications improve the accuracy of the COCAL code. In Table II, grid setups for the computations are listed. The grids H1–H4 correspond to different levels of resolutions. At each level, the resolution is double the previous one.[1]

In Figs. 2–4, the fractional errors in the lapse that are averaged over the angular coordinate grids (θ_i, ϕ_j) at fixed radial coordinate r are plotted against r of each coordinate patch,

$$\left\langle \left| \frac{\delta\alpha}{\alpha} \right| \right\rangle := \frac{1}{\#(\mathcal{G}_i)} \sum_{p \in \mathcal{G}_i} \left| \frac{\alpha - \alpha_{\rm exact}}{\alpha_{\rm exact}} \right|, \tag{14}$$

where writing a grid point (r_i, θ_j, ϕ_k) by p, we define a set $\mathcal{G}_i$ by $\mathcal{G}_i := \{p | p \in V \setminus S_e^{\rm in}$ and $r_i = {\rm const}\}$, where $S_e^{\rm in}$ is an interior domain of S_e, and $\#(\mathcal{G}_i)$ is the number of points included in $\mathcal{G}_i$.

In the top panel of Fig. 2, the same finite difference scheme as presented in Paper I is used for computing closer BBH solution with the BH excision radii $r_a = 0.2$ and 0.4, and with the separation $d_s = 2.5$. The midpoint rule in the θ integration is 2nd order accurate in this panel. In the bottom panel, the 4th order midpoint rule [Eq. (13)] for the θ integration is used for the same model and the same grid spacings. Clearly, the fractional error

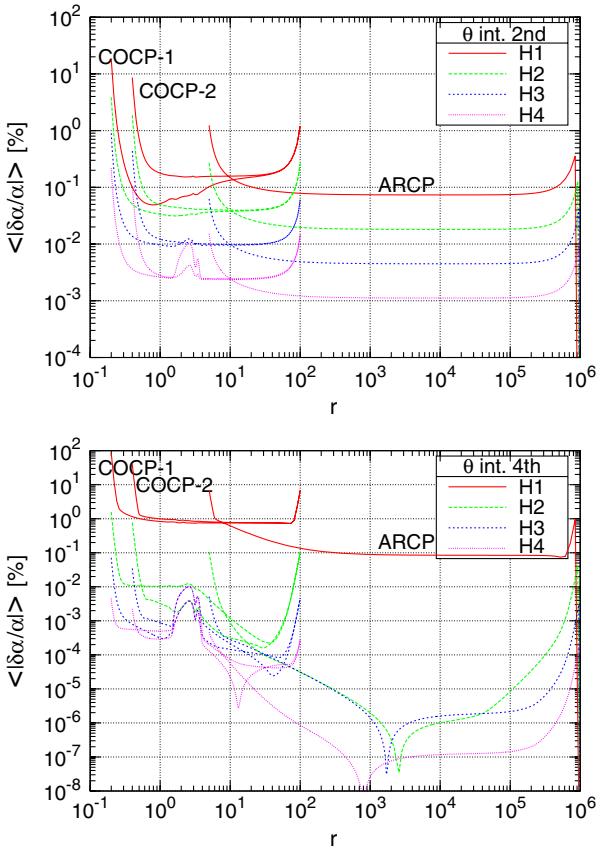

FIG. 2 (color online). Angular averaged fractional errors in the lapse $\langle|\delta\alpha/\alpha|\rangle$ are plotted along the radial coordinate r for the nonequal mass BBH data computed on three multiple patches. Top panel: data computed with the same coordinate grid spacings and finite difference schemes as in Paper I. Bottom panel: data computed with the 4th order θ integration discussed in Sec. II B 2. The grid parameters and number of grid points are varied as H1–H4 in Table II. The BH excision radii are chosen to be $r_a = 0.2$ and 0.4 for COCP-1 and 2, respectively, and the separation is to be $d_s = 2.5$.

[1]We have also tested different combinations of grid numbers (N_r, N_θ, N_ϕ) for the first level of resolution and performed convergence tests. We found the combination of type H was better than others. For example, the accuracy was not improved by increasing the grid points in the ϕ direction.

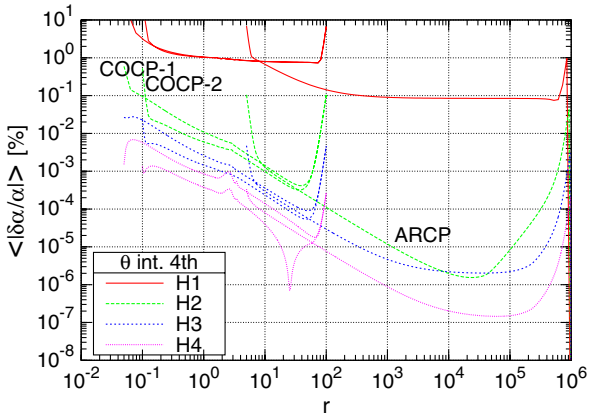

FIG. 3 (color online). Same as Fig. 2, but for the BH radius $r_a = 0.05$ and 0.1 for COCP-1 and 2, respectively. The results are calculated using the 4th order midpoint rule for θ integration as in the bottom panel of Fig. 2, otherwise the same finite differencing scheme (in particular, the same radial grid spacing Δr_i) as in Paper I.

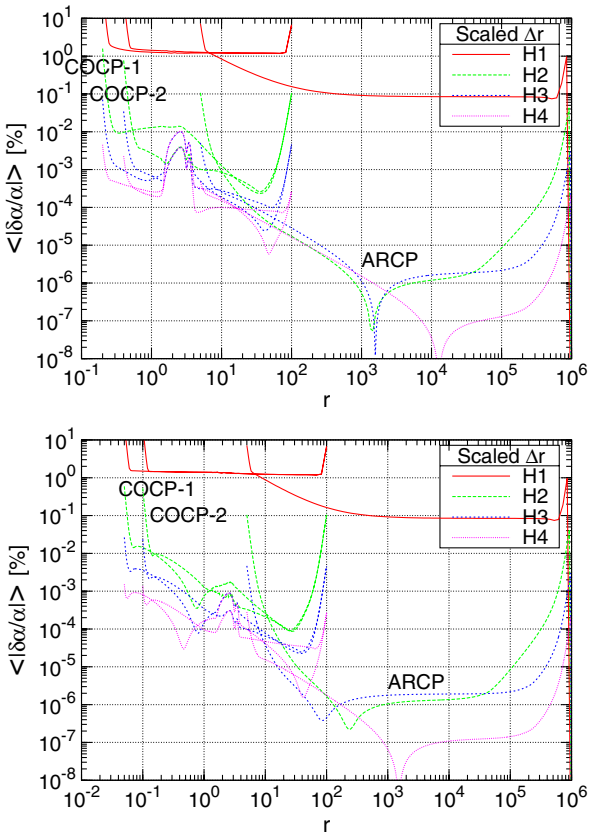

FIG. 4 (color online). Same as Fig. 2. The results are calculated using 4th order integration in θ coordinate Eq. (13), and the scaled radial spacing discussed in Sec. II B 1. Top panel: data with the BH radius $r_a = 0.2$ and 0.4 for COCP-1 and 2, respectively. Bottom panel: data with the BH radius $r_a = 0.05$ and 0.1 for COCP-1 and 2, respectively.

substantially decreases by this change for the H2 to H4 levels. We notice that the error near the BH converges in 4th order, that is, the error decreases about 1/16 at each level of resolution. The errors near the BH as well as in the asymptotic region are dominated by those from the θ integrations of the surface integral terms.

In Fig. 3, we calculate more separated BBH solutions, decreasing the radius of BH excision surface to 1/4 (therefore effectively separating BBH 4 times apart) as $r_a = 0.05$ and 0.1 with the same separation $d_s = 2.5$, and using the 4th order integration in θ as in the bottom panel of Fig. 2. Although the errors near the BH excision surfaces are of the same order of magnitude as those of the corresponding resolutions plotted in Fig. 2, bottom panel, the errors once increase as the radial coordinate r increases. It turns out that the BBH initial data discussed later cannot be calculated accurately with this grid setup for largely separated orbits.

In Fig. 4, convergence tests for the close ($r_a = 0.2$ and 0.4) and the separated ($r_a = 0.05$ and 0.1) BBH are calculated with scaled radial spacing near the BH introduced in Sec. II B 1, as well as the 4th order midpoint rule in θ integration. The size of the errors around the BH excision radius for the largely separated BBH data (bottom panel) is now comparable to those for the close BBH data (top panel) for each level of resolution. This improvement turns out to be important for accurately computing the separated BBH data in COCAL code.

III. COMPARISON OF BBH INITIAL DATA

A. The KADATH library

In this section, we compare the circular solutions of BBH initial data on a conformally flat spacelike hypersurface calculated from COCAL and the KADATH library. KADATH [7] is a library designed to solve a wide class of problems in theoretical physics including those of general relativity such as the above compact objects. It is based on spectral methods (see for instance [10] and references therein) where the various fields are approximated by finite sums of known functions typically trigonometrical functions and orthogonal polynomials. One of the main advantages of spectral methods is their fast convergence to the true solution (typically exponentially), when one increases the order of the expansion. For instance, in this paper, a relative accuracy of about 10^{-4} is achieved with 15 coefficients in each dimension.

Spectral methods enable one to translate a set of partial differential equations into an algebraic system on the coefficients of the expansions. This system is then solved by a standard Newton-Raphson iteration. The computation of the Jacobian as well as its inversion are parallelized.

The code used in this paper is essentially the same as the one used in Sec. 7.3 of [7]. In order to check the overall accuracy of the computations, one monitors the convergence of some global quantities (like the orbital frequency),

as a function of N, the number of points in each dimension. Let us mention that, in the case of a large separation, the code was slightly modified to maintain accuracy, probably due to a stretch of the bispherical coordinates when the distance between the holes gets much bigger than the size of the holes themselves. In particular, a spherical shell was added between the bispherical coordinates and the outer compactified domain and the determination of the orbital velocity had to be changed (see Sec. III C).

B. Conformally flat BBH initial data

The circular solution of BBH initial data is calculated by solving the Hamiltonian and momentum constraints, and the spatial trace of the Einstein's equation on a conformally flat spacelike hypersurface Σ_t. The spacetime metric on Σ_t is written in $3+1$ form as

$$\begin{aligned} ds^2 &= g_{\mu\nu}dx^\mu dx^\nu \\ &= -\alpha^2 dt^2 + \gamma_{ij}(dx^i + \beta^i dt)(dx^j + \beta^j dt), \end{aligned} \tag{15}$$

where the spatial three metric γ_{ij} on the slice Σ_t is assumed to be $\gamma_{ij} = \psi^4 f_{ij}$. Here, field variables ψ, α, and β^i are the conformal factor, lapse, and shift vector, respectively, and f_{ij} is a flat three-dimensional metric. We also assume maximal slicing to Σ_t, so that the trace of the extrinsic curvature $K_{ij} := -\frac{1}{2\alpha}(\mathcal{L}_t\gamma_{ij} - \mathcal{L}_\beta\gamma_{ij})$ vanishes. Writing its tracefree part A_{ij}, the conformally rescaled quantity $\tilde{A}_{ij}$ becomes

$$\tilde{A}_{ij} = \frac{1}{2\alpha}\left(\partial_i\tilde{\beta}_j + \partial_j\tilde{\beta}_i - \frac{2}{3}f_{ij}\partial_k\tilde{\beta}^k\right), \tag{16}$$

where the derivative ∂_i is associated with the flat metric f_{ij}, and conformally rescaled quantities with tilde are defined by $\tilde{A}_i{}^j = A_i{}^j$ and $\tilde{\beta}^i = \beta^i$, whose indexes are lowered (raised) by f_{ij} (f^{ij}). The system to be solved, which are Hamiltonian and momentum constraints and the spatial trace of the Einstein's equation, becomes

$$\Delta\psi = -\frac{\psi^5}{8}\tilde{A}_{ij}\tilde{A}^{ij}, \tag{17}$$

$$\Delta\beta_i = -2\alpha\tilde{A}_i{}^j\partial_j\ln\frac{\psi^6}{\alpha} - \frac{1}{3}\partial_i\partial_j\tilde{\beta}^j, \tag{18}$$

$$\Delta(\alpha\psi) = \frac{7}{8}\alpha\psi^5\tilde{A}_{ij}\tilde{A}^{ij}, \tag{19}$$

where $\Delta := \partial_i\partial^i$ is a flat Laplacian [2,11,12].

For the boundary conditions at the BH excision boundary S_a, we choose approximate irrotational apparent horizon boundary conditions,

$$\left.\frac{\partial\psi}{\partial r} + \frac{\psi}{2r}\right|_{r=r_a} = -\frac{\psi^3}{4}K_{ij}s^is^j, \tag{20}$$

$$\beta^i|_{r=r_a} = \frac{n_0}{\psi^2}s^i + \Omega y^i_{\rm cm}, \tag{21}$$

$$\alpha|_{r=r_a} = n_0, \tag{22}$$

where n_0 is an arbitrary positive constant for which we choose $n_0 = 0.1$, s^i is the unit normal to the sphere S_a, and Ω represents a parameter for orbital angular velocity. The vector $y^i_{\rm cm} := (0, d, 0)$ is the translational vector with respect to the center of mass. With these conditions, the sphere S_a becomes an apparent horizon (AH) in quasiequilibrium [5,7,13].

At the asymptotics, the boundary conditions are

$$\psi|_{r\to\infty} = 1.0, \tag{23}$$

$$\beta^i|_{r\to\infty} = 0.0, \tag{24}$$

$$\alpha|_{r\to\infty} = 1.0. \tag{25}$$

When using KADATH, the whole spacelike slice Σ_t is compactified, and hence the above conditions are imposed at the spatial infinity, while in COCAL, the computational domain is truncated at the radius $r_b \sim O(10^6$ M) and it is at r_b that the above conditions are imposed.

C. Comparison of the circular solutions of BBH initial data for KADATH and COCAL

Following [14], we obtain the angular velocity Ω of a circular orbit of BBH initial data from an assumption that an equality of Arnowitt-Deser-Misner (ADM) mass and Komar mass, $M_{\rm ADM} = M_{\rm K}$, is satisfied for the circular orbit, where $M_{\rm ADM}$ and $M_{\rm K}$ are defined by

$$\begin{aligned} M_{\rm ADM} &= \frac{1}{16\pi}\int_{S_\infty}(f^{ac}f^{bd} - f^{ab}f^{cd})\partial_b\gamma_{cd}dS_a \\ &= -\frac{1}{2\pi}\int_{S_\infty}D^a\psi dS_a, \end{aligned} \tag{26}$$

$$M_{\rm K} = -\frac{1}{4\pi}\int_{S_\infty}\nabla^\alpha t^\beta dS_{\alpha\beta} = \frac{1}{4\pi}\int_{S_\infty}D^a\alpha dS_a. \tag{27}$$

In COCAL, the surface integrals are calculated at a certain finite radius, typically around $r \sim (10^4$ M).

In KADATH, these integrals are usually evaluated at spatial infinity as its definition, $\int_{S_\infty} := \lim_{r\to\infty}\int_{S_r}$ with S_r the sphere of radius r. However, in the case of a large separation, it turned out that this was not giving good results. The precision of the results, measured by convergence of the value of Ω, is much better when one demands that, at spatial infinity,

$$1 - \alpha\Psi^2 \to \mathcal{O}(r^{-2}). \tag{28}$$

The difference between the Komar and ADM mass is then of the order of 10^{-4} for the higher resolution, thus giving a measure of the overall error of the code.

TABLE III. Comparison of BBH initial data from COCAL and KADATH for the cases $d_s/r_a = 12$ and $d_s/r_a = 30$. Fractional differences in % between the highest resolution cases of KADATH and COCAL are shown in the lines indicated by "Error". A column "Res." stands for the resolution.

Code	Res.	$\Omega M_{\rm irr}$	$M_{\rm ADM}/M_{\rm irr}$	$J/M_{\rm irr}^2$	$M_{\rm irr}/r_a$
			$d_s/r_a = 12$		
KADATH	11	0.127171	0.982866	0.757608	3.93366
KADATH	13	0.127299	0.983041	0.758390	3.93405
KADATH	15	0.127346	0.983072	0.758698	3.93417
COCAL	H2	0.127243	0.982848	0.754592	3.93191
COCAL	H3	0.127383	0.983125	0.758389	3.93392
Error [%]	···	0.03	0.005	0.04	0.006
			$d_s/r_a = 30$		
KADATH	11	0.0433696	0.933609	1.129241	3.56317
KADATH	13	0.0350000	0.988279	0.906819	3.55178
KADATH	15	0.0349704	0.988129	0.907249	3.55166
COCAL	H2	0.0344185	0.987369	0.889918	3.54574
COCAL	H3	0.0348624	0.987982	0.903226	3.55021
Error [%]	···	0.3	0.01	0.4	0.04

For a converged circular solution, we also calculate ADM angular momentum:

$$J = -\frac{1}{8\pi}\int_{S_\infty} K^a{}_b \phi^b dS_a. \tag{29}$$

The above quantities are normalized by the irreducible mass of AH, $M_{\rm irr}$, which is defined from the surface area of AH, namely, the area integral over the BH excision surface S_a,

$$A_{\rm AH} = \int_{S_a} \psi^4 r_a^2 d\Omega. \tag{30}$$

We write $M_{\rm irr1} := \sqrt{A_{\rm AH1}/16\pi}$ and $M_{\rm irr2} := \sqrt{A_{\rm AH2}/16\pi}$ for each BH, and write $M_{\rm irr} = M_{\rm irr1} + M_{\rm irr2}$ for a total mass.

In Table III, global quantities normalized by $M_{\rm irr}$ are presented for the irrotational BBH data computed from KADATH and COCAL at the separations $d_s/r_a = 12$ and $d_s/r_a = 30$. Three different resolutions for KADATH are given, mainly 11, 13, and 15 points in each dimension, and two (lower and higher) resolutions, H2 and H3, are used for the computations of COCAL. The relative differences between the highest resolution results from both codes are also indicated. The convergence of these quantities is plotted in Fig. 5 for both separations, $d_s/r_a = 12$ (left panels) and $d_s/r_a = 30$ (right panels). All plots indicate a nice convergence of the global quantities, when the resolutions are increased.

In Fig. 6, plotted are fractional errors of metric potentials of the same BBH data between those calculated from KADATH and COCAL. The errors are defined by $100 \times |q(\text{cocal}) - q(\text{KADATH})|/|q(\text{KADATH})|[\%]$, and those of the conformal factor ψ, lapse α, and y component of the shift β_y are plotted along the x axis which intersects

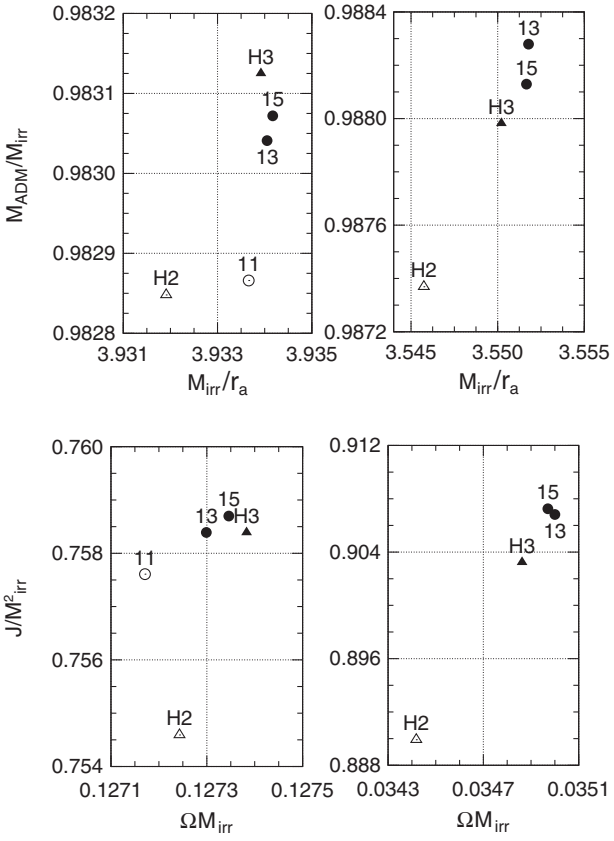

FIG. 5. The panels show the scaled values of $M_{\rm ADM}/M_{\rm irr}$ as a function of $M_{\rm irr}/r_a$ and $J_{\rm ADM}/M_{\rm irr}^2$ as a function of $\Omega M_{\rm irr}$. The circles denote the results from KADATH and the triangles the ones from COCAL. The runs using KADATH are labeled by the number of points in each dimension. The left top and bottom panels correspond to a separation of $d_s/r_a = 12$ and the right ones to $d_s/r_a = 30$ (in this case the lower resolution results from KADATH are outside the range of the plot).

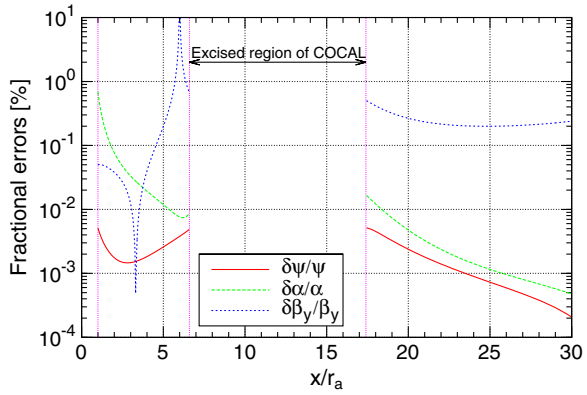

FIG. 6 (color online). Fractional errors in metric potentials between those calculated by KADATH and COCAL. Errors in the conformal factor ψ, lapse α, and y component of the shift β_y are plotted along the x axis that intersects with the centers of two BHs. The model is the same as that in Table III with the separation $d_s/r_a = 12$.

with the centers of two BHs for the case with the separation $d_s/r_a = 12$. Resolutions are H3 for COCAL and 15 points for KADATH. As seen from the figure, the metric potentials from the two codes agree well. Note that the relatively large error in β_y near $x/r_a \approx 6$ is due to β_y crossing zero, and hence its fractional error diverges there.

D. Solution sequence for corotating BBH data

Finally, we present a sequence of solutions for the conformally flat BBH initial data computed from COCAL.

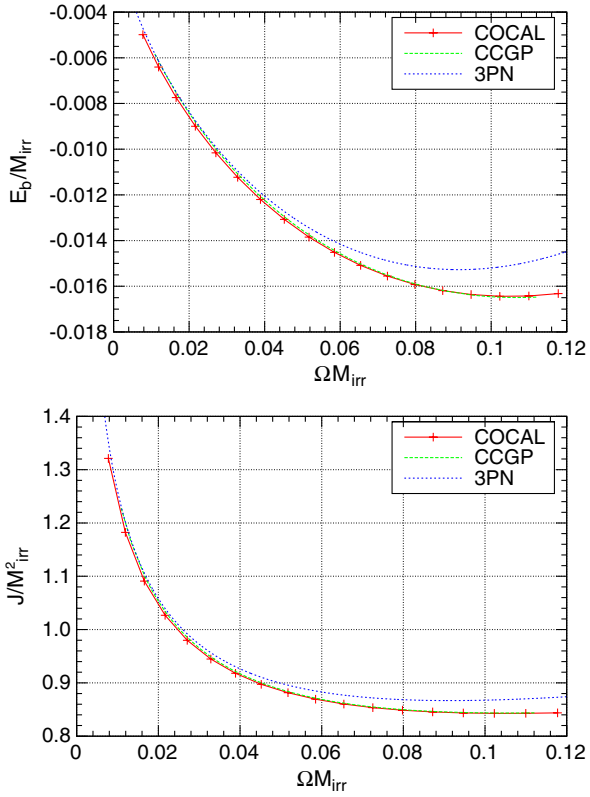

FIG. 7 (color online). Sequence of solutions for conformally flat BBH initial data with corotating spins are plotted. The sequence computed from COCAL code is compared with those presented in Caudill *et al.* [5] (CCGP) and with the third post-Newtonian (3PN) results [15].

TABLE IV. Solution sequence of equal mass BBH with corotating spins. In the computation, parameters H3 listed in Table II are used with a fixed separation $d_s = 2.5$, and with varying the excision radius r_a of BH.

r_a	d_s/r_a	$d_s/M_{\rm irr}$	$\Omega M_{\rm irr}$	$M_{\rm ADM}/M_{\rm irr}$	$E_b/M_{\rm irr}$	$J/M_{\rm irr}^2$	$M_{\rm irr}$
0.03	83.333	24.327	0.0077690	0.99501	−0.0049873	1.3211	0.10277
0.04	62.500	18.126	0.011925	0.99360	−0.0064032	1.1824	0.13793
0.05	50.000	14.403	0.016575	0.99226	−0.0077416	1.0910	0.17357
0.06	41.667	11.921	0.021647	0.99100	−0.0089952	1.0268	0.20972
0.07	35.714	10.147	0.027086	0.98984	−0.010159	0.97988	0.24638
0.08	31.250	8.8151	0.032848	0.98877	−0.011228	0.94470	0.28360
0.09	27.778	7.7785	0.038898	0.98780	−0.012201	0.91792	0.32140
0.10	25.000	6.9483	0.045207	0.98693	−0.013074	0.89736	0.35980
0.11	22.727	6.2682	0.051746	0.98615	−0.013847	0.88156	0.39884
0.12	20.833	5.7007	0.058495	0.98548	−0.014518	0.86946	0.43854
0.13	19.231	5.2197	0.065430	0.98491	−0.015087	0.86032	0.47896
0.14	17.857	4.8067	0.072533	0.98445	−0.015555	0.85355	0.52011
0.15	16.667	4.4481	0.079787	0.98408	−0.015922	0.84873	0.56204
0.16	15.625	4.1337	0.087174	0.98381	−0.016191	0.84550	0.60479
0.17	14.706	3.8557	0.094679	0.98364	−0.016362	0.84360	0.64839
0.18	13.889	3.6081	0.10229	0.98356	−0.016439	0.84279	0.69289
0.19	13.158	3.3860	0.10998	0.98358	−0.016424	0.84290	0.73834
0.20	12.500	3.1856	0.11775	0.98368	−0.016320	0.84377	0.78477

In this computation, the boundary condition of shift β^i (21) is replaced by that for the BBH with corotating spins,

$$\beta^i|_{r=r_a} = \frac{n_0}{\psi^2} s^i - \Omega \phi^i_{\rm cm}, \tag{31}$$

where the vector $\phi^i_{\rm cm}$ is a generator of rotation around the center of mass whose components in Cartesian coordinates is written $\phi^i_{\rm cm} = (-y_{\rm cm}, x_{\rm cm}, 0)$. The orbital angular velocity parameter Ω is evaluated with the same method as mentioned in the previous section.

In Fig. 7, a sequence of the corotating BBH data computed from COCAL with resolution H3 is compared with those of the paper by Caudill *et al.* [5], and of the third post-Newtonian (3PN) circular orbits [15]. In the top panel, the binding energy normalized by the irreducible mass $E_b/M_{\rm irr} := (M_{\rm ADM} - M_{\rm irr})/M_{\rm irr}$ is plotted against the normalized angular velocity $\Omega M_{\rm irr}$, and similarly in the bottom panel, the angular momentum $J/M^2_{\rm irr}$. The curves calculated from COCAL agree well with the other two curves. In the smaller $\Omega M_{\rm irr}$ (large separation), the curves from the COCAL are slightly smaller than those of the other works. The size of this error is comparable to that listed in Table III. The error in $E_b/M_{\rm irr}$ for the model with $d_s/r_a = 30$ is around -1.2% whose separation corresponds to the one in Fig. 7 with $\Omega M_{\rm irr} \sim 0.026$ ($d_s/r_a = 31.25$). The data used in Fig. 7 are tabulated in Table IV.

For computing a solution with the COCAL code, each iteration takes about 3 minutes for H3 resolution with a single CPU (1 core) of xeon X5690 3.46 GHz, and each run uses about 6GB of random-access memory. A convergence to a circular solution is achieved after 500–700 iterations, during which an iterative search for the circular Ω is made 5–7 times.

IV. DISCUSSION

We have presented additional convergence tests of COCAL code focusing on the BBH data. Especially the conformally flat initial data of BBH in circular orbit calculated from COCAL code are compared with those from KADATH code. We demonstrated that the results from both codes converge toward each other for large and small separations (see also [16]).

As fully discussed in [5], a corotating sequence presented in Sec. III D is not considered as a model for inspiraling BBH, because BBH tides do not effectively work to spin up the BH to synchronize the BH spin with orbital motion within the time of inspirals. In [5], the authors describe a more realistic sequence of BBH inspiral where the spin angular momentum of the AH is conserved. We will present elsewhere the performance of the COCAL code for computing those sequences to model BBH inspirals, which is a necessary step to compute more complex binary systems including black hole-neutron star binaries.

ACKNOWLEDGMENTS

This work was supported by JSPS Grant-in-Aid for Scientific Research(C) 23540314 and 22540287, and MEXT Grant-in-Aid for Scientific Research on Innovative Area 20105004. We thank Eric Gourgoulhon for discussion. K. U. thanks Charalampos Markakis, and Noriyuki Sugiyama for discussion.

[1] N. Stergioulas, Living Rev. Relativity **6**, 3 (2003), http://www.livingreviews.org/lrr-2003-3; R. Meinel, M. Ansorg, A. Kleinwächter, G. Neugebauer, and D. Petroff, *Relativistic Figures of Equilibrium* (Cambridge University Press, New York, 2008).

[2] G. B. Cook, Living Rev. Relativity **3**, 5 (2000), http://www.livingreviews.org/lrr-2000-5.

[3] H. P. Pfeiffer, Classical Quantum Gravity **29**, 124004 (2012).

[4] G. B. Cook, Phys. Rev. D **50**, 5025 (1994); S. Brandt and B. Brügmann, Phys. Rev. Lett. **78**, 3606 (1997); T. W. Baumgarte, Phys. Rev. D **62**, 024018 (2000);H. P. Pfeiffer, S. A. Teukolsky, and G. B. Cook, Phys. Rev. D **62**, 104018 (2000); P. Marronetti and R. A. Matzner, Phys. Rev. Lett. **85**, 5500 (2000); G. B. Cook, Phys. Rev. D **65**, 084003 (2002); H. P. Pfeiffer, G. B. Cook, and S. A. Teukolsky, Phys. Rev. D **66**, 024047 (2002); G. Lovelace, R. Owen, H. P. Pfeiffer, and T. Chu, Phys. Rev. D **78**, 084017 (2008); M. Ansorg, Phys. Rev. D **72**, 024018 (2005); M. Ansorg, B. Bruegmann, and W. Tichy, Phys. Rev. D **70**, 064011 (2004); W. Tichy, B. Brügmann, M. Campanelli, and P. Diener, Phys. Rev. D **67**, 064008 (2003); B. J. Kelly, W. Tichy, M. Campanelli, and B. F. Whiting, Phys. Rev. D **76**, 024008 (2007); B. C. Mundim, B. J. Kelly, Y. Zlochower, H. Nakano, and M. Campanelli, Classical Quantum Gravity **28**, 134003 (2011); L. T. Buchman, H. P. Pfeiffer, M. A. Scheel, and B. Szilagyi, Phys. Rev. D **86**, 084033 (2012).

[5] M. Caudill, G. B. Cook, J. D. Grigsby, and H. P. Pfeiffer, Phys. Rev. D **74**, 064011 (2006).

[6] K. Uryu and A. Tsokaros, Phys. Rev. D **85**, 064014 (2012), Paper I.

[7] P. Grandclement, J. Comput. Phys. **229**, 3334 (2010), Paper II.

[8] T. Nozawa, N. Stergioulas, E. Gourgoulhon, and Y. Eriguchi, Astron. Astrophys. Suppl. Ser. **132**, 431 (1998).

[9] D. R. Brill and R. W. Lindquist, Phys. Rev. **131**, 471 (1963).

[10] P. Grandclement and J. Novak, Living Rev. Relativity **12**, 1 (2009), http://www.livingreviews.org/lrr-2009-1.

[11] J. Isenberg, Int. J. Mod. Phys. D **17**, 265 (2008); J. Isenberg and J. Nester, in *General Relativity and*

Gravitation, edited by A. Held (Plenum Press, New York, 1980), Vol. 1.

[12] J. R. Wilson and G. J. Mathews, in *Frontiers in Numerical Relativity*, edited by C. R. Evans, L. S. Finn, and D. W. Hobill (Cambridge University Press, Cambridge, England, 1989), p. 306.

[13] J. Thornburg, Classical Quantum Gravity **4**, 1119 (1987); S. Dain, Classical Quantum Gravity **21**, 555 (2004); **22**, 769(E) (2005).

[14] E. Gourgoulhon, P. Grandclement, and S. Bonazzola, Phys. Rev. D **65**, 044020 (2002); P. Grandclement, E. Gourgoulhon, and S. Bonazzola, Phys. Rev. D **65**, 044021 (2002).

[15] L. Blanchet, Living Rev. Relativity **9**, 4 (2006), http://www.livingreviews.org/lrr-2006-4; L. Blanchet, Phys. Rev. D **65**, 124009 (2002).

[16] A. Tsokaros and K. Uryū, J. Eng. Math. (to be published).